DOI: 10.1177/0954407020940824

Original Article

Institution of MECHANICAL ENGINEERS

Journal of AUTOMOBILE ENGINEERING

Proc IMechE Part D:
J Automobile Engineering
2021, Vol. 235(1) 245–259

DOI: 10.1177/0954407020940824
journals.sagepub.com/home/pid
SAGE

Diagnosis of hydrous ethanol combustion in a spark-ignition engine

Caio H Rufino[1], Waldyr LR Gallo[2] and Janito V Ferreira[3]

Abstract

By evaluating combustion duration and flame development, it is possible to evaluate the effects of utilizing a new type of fuel. This allows for optimization of the operational parameters such as the ignition timing, air–fuel ratio, and throttle opening with respect to efficiency, knock, emissions, and performance. In this work, the combustion of a Brazilian hydrous ethanol fuel was evaluated in a commercial flexfuel engine. Investigations were conducted by performing a heat release analysis of the experimental data and providing combustion characteristics. The experimental design comprised of variations in engine speed, load, ignition timing, and air–fuel ratio under lean condition. The results indicated the relationship between the engine parameters and combustion characteristics under a wide range of operational conditions, and identified the relationship between the physical characteristics of the fuels and their combustion in the commercial engine. For high engine speed, lean combustion presented a similar duration to the stoichiometric combustion duration. When comparing the combustion characteristics obtained for the hydrous ethanol with gasoline combustion, the main differences noted were reduced sensitivity to detonation and a shorter duration of combustion, although the temperature at the start of combustion was lower for ethanol. In addition to shorter combustion duration, ethanol presented a lower value for the Wiebe exponent. The results obtained from the combustion duration values and Wiebe function parameters enable the composition of a set of data required for a simplified combustion simulation.

Keywords

Mass fraction burned analysis, ethanol, flexfuel engines, Wiebe function parameters, spark-ignition engines

Date received: 3 February 2020; accepted: 4 June 2020

Introduction

Combustion diagnosis is a powerful tool employed in internal combustion engines, and it provides information regarding combustion characteristics using a thermodynamic approach. It is performed using the measured in-cylinder pressure, as it is the most accessible thermodynamic property in the cylinder.[1] The combustion effect on the in-cylinder pressure can be isolated from other phenomena such as blow-by, heat transfer, internal energy change, and work.[2] The outputs of the procedure are known as the apparent heat release (AHR) and the heat release rate (HRR) profiles. The start of combustion (SOC), end of combustion (EOC), and other secondary parameters such as the combustion duration, ignition delay, and form of combustion can be deduced from the AHR profile. Therefore, it is possible to perform this analysis to determine the effect on combustion from engine design parameters such as piston geometry, compression ratio, and valve timing, as well as operational parameter, which are constantly adjusted by an electronic control unit (ECU) during the operation of the engine, such as air–fuel ratio, spark timing and load. From the HRR profile, it is also possible to understand the effect of each tested parameter on the phases of combustion, specifically the flame development phase (usually the phase until 10% of the fuel is burnt), fast burn phase (burnt fuel is from 10% to 90%), and quenching phase.[3] Much research has been conducted on spark ignition engines (SIs), and it is possible to derive the mass fraction burned (MFB) from the AHR profile by knowing the trapped mass in the cylinder and the

[1]Laboratory of Biofuel Engines, School of Mechanical Engineering, University of Campinas, Campinas, Brazil
[2]Department of Energy, School of Mechanical Engineering, University of Campinas, Campinas, Brazil
[3]Department of Computational Mechanics, School of Mechanical Engineering, University of Campinas, Campinas, Brazil

Corresponding author:
Caio H Rufino, Laboratory of Biofuel Engines, School of Mechanical Engineering, University of Campinas, 13083-970 Campinas-SP, Brazil
Email: rufino119186@gmail.com

energetic content of the fuel, thereby providing a value for the fraction of burned fuel along the engine cycle.[4]

Other methods can characterize combustion from a more detailed and microscopic approach. For example, the flame growth, structure, and speed can be measured in optical engines or closed vessels to obtain the effects of specific parameters on combustion, for example, the air–fuel ratio,[5] diluent concentration[6] and temperature.[7] Such analyses can also be used to present comparisons between different types of fuels.[8,9] However, determining the effect of the combined variation of many parameters within the wide operational conditions of an engine can be a difficult task. Thus, combustion diagnosis is still a reliable tool for characterizing combustion, and can be used in parallel to those methods, based on a more theoretical approach. Moreover, combustion diagnosis can provide data for data-based MFB models for engine simulation. The most frequently used correlation that describes the MFB profile is the Wiebe function.[10] Consequently, several studies in combustion diagnosis have evaluated combustion characteristics by fitting the parameters of the Wiebe function to the studied case.[3,11–13]

Many implementations of combustion diagnosis can be found in the literature, such as a study on effects of a secondary injection of natural gas on compression-ignition (CI) engines[14] or a study on the effects of using blends of ethanol and n-butanol in diesel.[15] Some investigations suggest the implementation of such models on real-time diagnosis to assist engine control, such as determining the beginning of combustion in CI engines[16] or the combustion duration in SI engines.[17]

Other examples of application for combustion diagnosis include the simulation of homogeneous charge compression ignition and spark assisted compression ignition, in which the model must consider the effects of auto-ignition together with flame propagation,[18] in addition to experimental exergetic analysis,[19] calibration of predictive simulation models for engines,[1] and educational purposes, such as engineering education.[20]

Bioethanol is a promising alternative as a substitute for fossil fuels,[21] and the development of engines adapted for this fuel relies on fuel characterization, which can be performed through combustion diagnosis. In addition to being produced from renewable sources, ethanol presents a higher heat of vaporization and faster flame speed, leading to a higher resistance to knock onset, thus facilitating downsizing through turbocharging.[21,22] Moreover, the presence of oxygenates contributes to flame stability, resulting in a reduction of carbon monoxide and hydrocarbons emission.[23] As examples of research, studies performed on ethanol usage in internal combustion engines one can cite evaluations of anhydrous and hydrous ethanol combustion in port fuel injection (PFI) and direct injection (DI) engines,[24] the effects of spark advance and compression ratio on gasohol blends,[25] and effect of water content on DI engines.[26] Studies on the performance, emission, and combustion characterization of engines operating with hydrous ethanol, gasohol blends, and wet ethanol (ethanol with high water content) were summarized in a review by El-Faroug et al.[27]

Currently, the Brazilian market offers hydrous ethanol and gasohol, which are referred to in this paper as E95h and E27, respectively. Only a few studies have evaluated the operation of Brazilian hydrous ethanol in flexfuel engines. For example, Costa and Sodré compared gasohol and hydrous ethanol operations in terms of their brake specific consumption, thermal efficiency, and emission in a wide range of speed under full load conditions.[28] Subsequently, the authors studied the effects of the compression ratio for a flexfuel engine operating with ethanol on the specific fuel consumption, brake mean effective pressure, brake power, brake torque, and thermal efficiency under the same conditions as the previous study.[29] Another study was conducted by Melo et. al., who measured the brake thermal efficiency and emissions in a flexfuel engine operating at a constant torque under different speed conditions.[30] Further investigations of the same engine were performed to evaluate the effects of hydrous ethanol and gasohol blends on knock, cyclic variability, and combustion duration at a constant torque and under three-speed conditions.[31] Another investigation expanded the cited study by evaluating the effects of hydrous ethanol and gasohol blends on heat release and emissions under two-load conditions and at three speeds under stoichiometric and rich conditions.[32] In these studies, the evaluations were performed either under a full load or specific load condition, the air–fuel ratio was set to either a stoichiometric condition or a rich condition, and the spark advance was set to either maximum brake torque (MBT) or limited knock. Moreover, there were no data related to the effect of the air–fuel ratio under a lean condition and only a limited range of data can be found for analysis on the effect of load. The use of ethanol does not limit itself for the Brazilian transportation sector. Sileghem et al.[33] discussed that the use of biofuels and their blends with gasoline should be interpreted as an evolution. They cited the European market, in which ethanol is currently being used as mean for improving fuel octane number, and the North American market, in which the E85 fuel is used.

This work contributes to the literature by presenting a combustion diagnosis of E95h on a commercial SI PFI flexfuel engine in the context of a two zone heat release model. The objectives of this study consist of evaluating the effects of engine parameters on hydrous ethanol combustion, correlating those effects to studies found in the literature and indicating the degree of influence of each engine parameter. Moreover, a comprehensive set of results provides an experimental data for modeling hydrous ethanol combustion in a flexfuel engine simulation. Thus, experiments were conducted in a wide range of operational conditions for engine speed, throttle position and ignition timing. In some cases, the calibration strategy of the ECU for the commercial engine was preserved. In addition, there is a scarcity of results regarding the combustion characteristics of an air–fuel ratio in a lean condition; this topic is also covered by this work. Although the catalyst operation limits the air–fuel ratio to stoichiometric and rich conditions, lean mixtures have been considered for partial load operations with the objective of reducing pumping losses.[22] This is because the combustion stability of ethanol enables operation at lean conditions without significantly reducing the vehicle drivability.[23] The characteristics of combustion were indicated by the values of the Wiebe function parameters: combustion duration, form factor, 50% of MFB and combustion phases duration, which are presented in the Methodology section. A comparison of E95h with gasohol E27 was also performed to determine the differences between the characteristics of both fuels combustion. The method used to perform the heat release analysis is also described in the Methodology. Descriptions of the experimental setup and the tests are provided in Experimental setup section. The section Results discloses and discusses the results. The inferences obtained from the evaluation results are summarized in the Conclusion.

Methodology

The pioneer method for determining heat release from experimental data was developed by Rasswiler and Withrow (RW), and consists of correlating the MFB to the pressure rise fraction caused by the combustion.[34] A more elaborated method was proposed by Krieger and Borman (KB), as described by Gatowski et al.,[2] and is based on the energy conservation law as applied to the in-cylinder gases, allowing for the inclusion of heat transfer and blow-by effects. A comparison between the methods was conducted by Brunt and Emtage,[35] which demonstrated that the KB method provides higher reliability and accuracy. However, when the amount of heat release is low, that is, in a partial-load condition, the RW method presents more robustness to noise and uncertainties owing to its simplicity, and it remains preferred by some researchers to date. Many researchers have expanded both methods to a two-zone approach, in which reactants and combustion products are analyzed separately. Stone et al.[36] and Ball et al.[37] have described two-zone models based on the RW method. Only few combustion diagnosis methods were based on the two–zone approach. This approach consists of separately applying the energy conservation law to reactants and to combustion products.[1,38,39] A higher accuracy and the possibility of obtaining temperature profiles for reactants and products are the main advantages of implementing the two–zone diagnosis model.

In this work, a two–zone model was developed and implemented to conduct the combustion diagnosis and thereby to obtain the MFB profile. The parameters evaluated in the analysis are obtained from the MFB profile, such as SOC, CA10, CA50, CA90, EOC, combustion duration, n and ignition delay. All these parameters were used to evaluate the behavior of the combustion with respect to the operational conditions of the engine.

Heat release profile

First, the mass of a homogeneous mixture trapped in the cylinder is estimated by measuring the instantaneous fuel flow and air–fuel ratio. Although the intake manifold design can lead to a non-homogeneous distribution of mass, the adopted hypothesis (homogeneous mass distribution for all cylinders) is very close to that of SI engines, as reported by Depcik et al.[20]

Work and heat transfer are the only interactions of energy exchange in the cylinder prior to the ignition event. Hence, this part of the cycle can be used to estimate the temperature of the cylinder wall. The energy transfer via the work interaction occurs in the cylinder only because of the piston displacement, thus $\delta W = P\frac{dV}{d\theta}$. The internal energy depends only on temperature as a consequence of the ideal gas hypothesis. Therefore, the differential of internal energy is given by the differential of temperature times the specific heat of the mixture (c_v). Its value is fitted for all substances as a function of temperature, by using data provided by the National Institution of Standards and Technology thermophysical tables, and then it is calculated for the mixture. The reactants are considered to be a mixture of fuel and air. Dry air is modeled as an ideal gas composed of nitrogen, oxygen, carbon dioxide, and argon. Air humidity is measured at the location where the tests were performed.

The heat transfer δQ is obtained by isolating it from the energy balance and neglecting blow-by

$$\delta Q = P\frac{dV}{d\theta} + c_v\frac{dT}{d\theta} \tag{1}$$

The differential of the temperature is given by the following state equation

$$\frac{dT}{d\theta} = T\left(\frac{1}{P}\frac{dP}{d\theta} + \frac{1}{V}\frac{dV}{d\theta}\right) \tag{2}$$

By substituting equation (2) into equation (1) and rearranging the terms, the heat transfer profile is obtained as follows

$$\delta Q = P\left(\frac{c_v}{R} + 1\right)\frac{dV}{d\theta} + V\frac{c_v}{R}\frac{dP}{d\theta} \tag{3}$$

In the above, the constant R is the difference between specific heats at a constant pressure and constant volume. Once the in-cylinder gas is colder than the cylinder wall at the beginning of the compression stroke, and after closing the intake valve, the heat transfer occurs from the wall to the gas. Then, the gas is compressed and its temperature rises, changing the direction of the heat flux. Consequently, there is a moment in which the gas and the cylinder wall are at the same temperature, and this instant can be determined as the time when the heat flux is calculated as null. The cylinder walls temperature is defined in this instant as being the same as the in-cylinder gas temperature. Most works found in the literature arbitrarily estimate the cylinder walls temperature or adjust the temperature *ad hoc*. Although this information is not essential for a combustion diagnosis, it is fundamental for a second law analysis of experimental engine data.

The combustion energy released after the ignition cannot be differentiated from the heat transfer in the energy balance, and the equations provide the net heat release. To achieve a higher accuracy, many studies in the literature implement an estimate of heat transfer, thus separating the effects of combustion and heat losses, and obtain the gross heat release. In this analysis, the heat release is estimated from the convection law

$$\delta Q = \frac{h^{HT} A (T - T_w)}{\omega} \tag{4}$$

In the above, A is the heat transfer area of each zone and T_w is the cylinder wall temperature. The heat transfer coefficient h^{HT} is calculated as a function of volume, pressure, temperature and mean piston velocity, as suggested by Hohenberg.[40]

The two zone model consists of applying the energy conservation law to two zones: one formed by reactants (represented by the subscript r) and the other formed by combustion products (represented by the subscript p). The development of the model assumes that the gases do not mix, that the zones are at the same pressure and different temperatures, and that the zones are separated by the flame front.

The composition of combustion products is considered to be dependent on the stoichiometric condition. This model considers a fixed composition for combustion products. A complete combustion leads to a mixture of carbon dioxide, water, argon, and nitrogen if the stoichiometric condition ($\lambda = 1$) is achieved. For conditions of excess air, that is, a lean condition ($\lambda > 1$), oxygen is present in the combustion products. On the other hand, if the air is insufficient, that is,, the rich condition ($\lambda < 1$), then the combustion is incomplete. Thus, part of the carbon present in the fuel is converted into carbon monoxide, whereas a part of the hydrogen present in the fuel is converted into molecular hydrogen. It should be noted that the species balance does not provide a sufficient number of relationships to solve the stoichiometric balance. Thus, it is necessary to assume that a relationship exists between carbon monoxide and molecular hydrogen, based on an estimative of the chemical equilibrium between those substances.[41]

By applying the energy conservation law to reactants and using the relation between the internal energy U and enthalpy $H: \ U = H + PV$, it can be established

$$\frac{dH}{d\theta} = \delta Q + V\frac{dP}{d\theta} + h\frac{dm}{d\theta} \tag{5}$$

This equation can be applied for both zones, reactants and products. The enthalpy in the mass transfer term (h) is the enthalpy of reactants while the mass transfer rate is given by $\frac{dm}{d\theta} = -m\frac{dX_b}{d\theta}$ for reactants and $\frac{dm}{d\theta} = m\frac{dX_b}{d\theta}$ for combustion products, being X_b the MFB.

By separating the effects of mass and temperature on the extensive enthalpy of the gas as, it is possible to isolate the temperature differential for reactants

$$\frac{dT_r}{d\theta} = \frac{\delta Q_r + V_r\frac{dP}{d\theta}}{c_{p,r}(1 - X_b)m} \tag{6}$$

and for combustion products

$$\begin{aligned}\frac{dT_p}{d\theta} &= \left(c_{p,p}X_b m\right)^{-1}\Big\{\Big[m_{fuel}LHV + \\ &\quad m\left(c_{p,r}T_r - c_{p,p}T_p\right)\Big]\frac{dX_b}{d\theta} + \delta Q_p + V_p\frac{dP}{d\theta}\Big\}\end{aligned} \tag{7}$$

Here, the energy release by combustion is given by $m_{fuel}LHV\frac{dX_b}{d\theta}$ with the lower heating value LHV and the admitted mass of fuel m_{fuel} as calculated using the measured air–fuel ratio.

The rate of volume dislocation is given by

$$\frac{dV}{d\theta} = \frac{dV_r}{d\theta} + \frac{dV_p}{d\theta} \tag{8}$$

and by applying the ideal gas law, together with the temperature differentials obtained from the energy conservation law, it is possible to isolate the MFB

$$\begin{aligned}\frac{dX_b}{d\theta} &= \\ &\left[\frac{R_p}{c_{p,p}}\left(-\delta Q_p - V_p\frac{dP}{d\theta}\right) + P\frac{dV}{d\theta} + V\frac{dP}{d\theta} - \right. \\ &\left. m(1 - X_b)R_r\frac{dT_R}{d\theta}\right]\Big\{m\Big[R_pT_p - R_rT_r + \\ &\frac{R_p}{c_{p,p}}\left(\frac{m_{fuel}LHV}{m} + c_{p,r}T_r - c_{p,p}T_p\right)\Big]\Big\}^{-1}\end{aligned} \tag{9}$$

For those three differential equations, it is necessary to define an initial value to implement the Runge–Kutta method. The initial value for the MFB is null. The initial temperature value for the reactants is determined by the ideal gas model applied at the instant of intake valve closing, and the initial temperature for the first portion of the combustion products is considered to be the adiabatic flame temperature.

CA50

Once the profile of the released heat is determined, a criteria for specifying the start and EOC must be chosen. It was selected using a method based on identifying instants of 10, 50, and 90% of the MFB, also known as CA10, CA50, and CA90, respectively. These parameters are given by the integration of the HRR, that is, the heat released, which is smoother than the HRR (owing to the integration process).

Generally, the MFB is approximated by a function which describes the development of combustion. The researcher Ivan Wiebe developed a semi–empirical correlation for reproducing the effect of a complicated chemical reaction chain with a simple expression.[10] Thus, this developed model can reproduce the behavior of combustion, by adjusting a few parameters[34] calibrated with experimental data. It has been reported that each engine and condition can provide different parameters for this model. The function is given in equation (10)

$$X_b = 1 - \exp\left[\ln(1-\eta)\left(\frac{\theta-\theta_0}{\Delta\theta}\right)^{n+1}\right] \tag{10}$$

The above equation is commonly referred to in the literature as the Wiebe function.

The term η is the maximum value of the MFB and is dependent on the combustion efficiency. In this work, the combustion efficiency is estimated rather than calculated. This parameter is usually replaced by another parameter, $a = -\ln(1-\eta)$. Many authors have chosen arbitrary values for this parameter, a, which varies from 4 to 6.908.[3] The latter value was the pioneering suggestion of Wiebe,[10] and was reinforced by other authors.[12,42] That value is adopted for this work, and leads to a combustion efficiency of $\eta = 0.999$.

Moreover, the use of CA50 is fundamental for estimating the parameters $\Delta\theta$ (combustion duration) and n (form factor).

Form factor

In this study, the parameter n represents the form factor. The form factor indicates the degree of asymmetry of the combustion profile. The effects of this parameter on the burning profile can be verified from the works of Mueller et al.[34] and Gallo.[43] The higher the value of n, the slower the combustion will be at its beginning. In contrast, small values of n indicates that the combustion develops quickly, and that the fast burn region occurs early.

By substituting the obtained crank angles of CA10 (θ_{10}), CA50 (θ_{50}), and CA90 (θ_{90}) in θ and 0.1, 0.5, and 0.9 in X_b (equation (10)), respectively, it is possible to determine the SOC

$$\frac{\theta_{10}-\theta_0}{\theta_{90}-\theta_0} = \left(\frac{\theta_{50}-\theta_0}{\theta_{90}-\theta_0}\right)^{L} \tag{11}$$

in which the constant L is

$$L = \frac{\ln\left(\frac{\ln 0.9}{\ln 0.1}\right)}{\ln\left(\frac{\ln 0.5}{\ln 0.1}\right)} \tag{12}$$

Multiple roots can be found when solving equation (11) for θ_0 (SOC). Hence, the bisection method of numerical solving is implemented for the interval between the ignition and CA10. In most cases, the start of the combustion was given as the same instant as the ignition. In other cases, it was observed that there is a brief delay between the ignition and the SOC. This period of time is defined as the ignition delay.

The parameter n can be determined by the following:[13]

$$n = \frac{\ln\left(\frac{\ln 0.9}{\ln 0.1}\right)}{\ln\left(\frac{\theta_{10}-\theta_0}{\theta_{90}-\theta_0}\right)} \tag{13}$$

Combustion duration

One of the most fundamental parameters in the combustion analysis is the duration of combustion. This parameter is directly linked to the efficiency of the engine, and a faster combustion is preferred in most conditions. By using the developed equation, the combustion duration can be determined as follows:[13]

$$\Delta\theta = (\theta_{50}-\theta_0)\left(\frac{\ln 0.5}{1-\eta}\right)^{\frac{-1}{n+1}} \tag{14}$$

Experimental setup

The experimental tests were executed in the PSA's spark–ignition port fuel injection engine (Table 1). It includes three cylinders with an in–line configuration and a nominal compression ratio of 12.5:1. Although data were measured for all cylinders, it was arbitrarily opted to evaluate the data acquired for cylinder 1, whose measured compression ratio was 12.28:1. The tested engine was a multi–fuel engine, also known as a flexfuel engine. Flexfuel engines are widely used in light duty vehicles in Brazil and are capable of being fuelled by gasoline, hydrous ethanol, or even a blend of both fuels, composed of any proportions. The bench tests were executed at the Instituto Mauá de Tecnologia (IMT) facilities. A ETAS ECU for development was used to control the engine. The in–cylinder pressure was acquired by using instrumented spark plugs AVL

Table 1. Engine characteristics.

Cylinders	3 in line
Compression ratio	12.28:1
Connecting rod length [mm]	145.6
Displacement [cm^3]	1200
Bore [mm]	75
Stroke [mm]	90.5

Table 2. Test parameters.

	Full load	Ignition timing sweep	Lean mixture
Engine speed	1000–6000	1500 and 3000	1000–4000
λ	< 1	1	1–1.3
Load	Full	20–100%	25 and 50 Nm
Fuel	E27&E95h	E27&E95h	E95h

ZI31_Y5S. The tests were performed with a passive eddy current positron Brown-Boveri dynamometer.[44]

The fuels used in the test were those currently available in the Brazilian market for SIs: E95h and E27. E27, also known as gasohol, consists of a gasoline 86 MON/95 RON blended with 27% ethanol in volume. E95h, that is, hydrous ethanol, consists of a blend of 95% ethanol and 5% water in a volume of liquid. In all conditions, the engine was running under normal operational conditions. The experiments were separated into three categories: full load, ignition timing sweep and lean mixture (Table 2). It was not possible to obtain a stable engine operation for the condition of $\lambda = 1.3$ for 50 Nm of load. Thus, results are not provided for that specific condition.

Load is indicated by throttle position for the ignition timing sweep test, whereas it is indicated by torque for the lean mixture test (Table 2).

The air–fuel ratio was not controlled for the full load test, as it was at a rich condition during the entire test. The ignition timing was set either to the MBT condition or to knock limited for both the full load and lean mixture tests. The conditions of 25 and 50 Nm of load are representative of the vehicle's engine operation and they represent a different percentage of the torque at full load for different engine speed conditions, between 20% and 40% for 25 Nm and between 40% and 80% for 50 Nm.

Data processing consisted of averaging the obtained cycles for the in–cylinder pressure and the parameters used in the calculation of the released heat, such as the rate of fuel flow, ambient temperature, humidity, air-fuel ratio, and ambient pressure. In that regard, 300 cycles with a resolution of 0.5 ºCA were obtained for the full load and ignition sweep tests, whereas 150 cycles with a resolution of 0.2 ºCA were obtained for the lean mixture test. After averaging, the pressure profile was smoothed to eliminate noise and fluctuations caused by phenomena that were not modeled in the heat release analysis, e.g. charge motion and pressure waves caused by valve closing. In addition to those phenomena, noise can also influence the signal. When the measured signal was differentiated without signal processing for noise elimination, those fluctuations were amplified, decreasing the reliability of the diagnosis. Although digital filters (such as Butterworth filters), or smoothing techniques (such as Savitsky-Golay) are commonly used to perform signal processing for

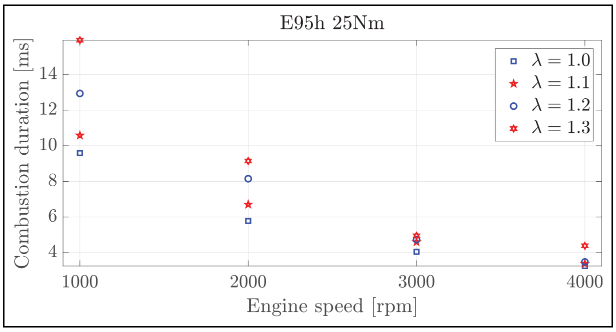

Figure 1. Combustion duration for different A/F ratios and engine speed at 25 Nm.

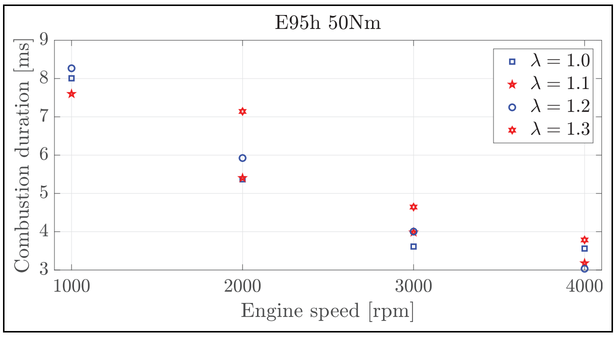

Figure 2. Combustion duration for different A/F ratios and engine speed at 50 Nm.

pressure data, it was decided to implement a new technique based on a support vector machine[45] as this method was proven to be more robust and reliable. A numerical differentiation of the fourth order was used to perform the pressure differentiation.

Results and discussion

The heat release profiles were obtained for the aforementioned experimental conditions. The combustion duration, *n* and ignition delay were calculated based on the heat release profile according to the method shown through equations (11)–14.

A/F ratio and load effects

The combustion duration decreases with increased engine speed owing to increased turbulence (Figure 1). However, in terms of ºCA, this trend could not be observed, as crank displacement is dependent to the engine's angular velocity. Therefore, an analysis for combustion duration in terms of time (milliseconds) is more appropriate.

The major contribution to flame speed comes from the turbulence,[22] which was easily verified from the significant decrease in combustion duration with an increase of engine speed (Figures 1 and 2). Although the flame is turbulent in engines, the laminar flame speed is a characteristic that can indicate the effect of

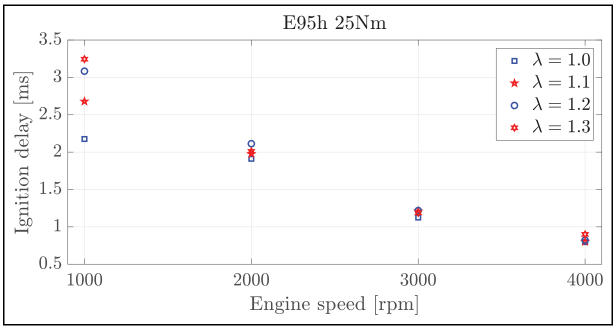

Figure 3. Ignition delay for different A/F ratios and engine speed at 25 Nm.

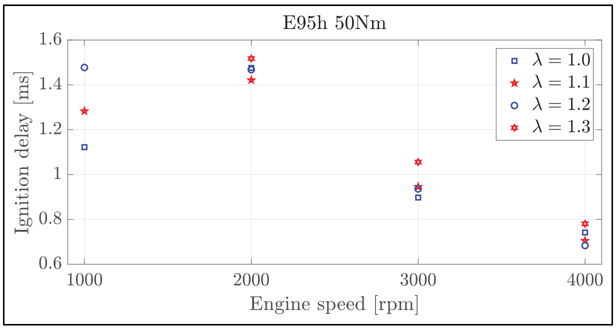

Figure 4. Ignition delay for different A/F ratios and engine speed at 50 Nm.

other parameters on combustion. The laminar flame speed is affected by the pressure, temperature and A/F ratio.[7] Eisazadeh-Far et al.[6] showed that the concentration of diluent gases also influences the laminar flame speed, by illustrating that a higher concentration of diluent gases induces a decrease of the adiabatic flame temperature, which decreases the flame speed. Varea et al.[46] and Gülder[8] showed that flame velocity is maximized for slightly rich mixtures. Moreover, studies have shown that the flame speed of ethanol is lower for a lean mixture as compared to that of a stoichiometric condition.[47] In the obtained results, the combustion duration did not present a strong relation to the A/F ratio, except for the condition of $\lambda = 1.3$, which presented a longer combustion duration than those of other A/F ratio conditions. This trend may be attributed to the fact that the stochastic nature of the turbulent flame can overlap the effect of the A/F ratio on the laminar flame speed. As the load control is performed by limiting the amount of trapped mass, the in–cylinder pressure is reduced for low loads. Therefore, a decrease in combustion duration is observed for 50 Nm as compared to that for 25 Nm (Figures 1 and 2), which agrees with the results found in the literature for engines fueled with gasoline[1,12] and gasohol.[48]

The ignition delay proved to be lower for higher loads (Figures 3 and 4), indicating the relationship between pressure and flame development. Moreover, the ignition delay decreased with increased engine speed. For low speeds, a higher level of sensibility to A/F ratio was observed in the ignition delay. Leaner A/F ratios induced a higher ignition delay, exposing the effects of diluent gases and low adiabatic flame temperature.

The parameter CA50 presented a shift from top dead center (TDC) for high values of λ as the combustion duration was increased for leaner mixtures. No relation between CA50 and engine speed was observed (Table 3) once the values were constant aside from minor fluctuations. The fixed value for CA50 is explained by the fact that the combustion duration reduction with engine speed was compensated for by the increasing angular velocity.

Combustion is divided into four main phases in this analysis: the flame development phase, defined as the period between the SOC and CA10; the beginning of the fast burn phase, defined as the period between CA10 and CA50; the end of the fast burn phase, defined as the period between CA50 and CA90; and the final phase, defined as the period between CA90 and the EOC. The fast burn period comprehends the period between CA10 and CA90. Absolute and normalized values are presented, that is, the ratio between each phase and the total combustion duration. Values are respectively provided for 25 and 50 Nm (Appendix 2, Tables 5 and 6).

Table 3. CA50 for different A/F ratios and engine speed.

Load	Engine speed (r/min)	λ			
25 Nm		1.0	1.1	1.2	1.3
	1000	8	10	15	18
	2000	10	13	17	19
	3000	8	10	13	16
	4000	9	10	14	19
50 Nm	1000	9	10	12	–
	2000	9	12	16	21
	3000	9	11	15	19
	4000	9	11	14	18

The stoichiometric condition presented the longest flame development phase for 25 Nm, except for 4000 r/min, where the turbulence effect overlapped the effect of the A/F ratio as previously mentioned. For 50 Nm, the effect of the load overlapped the effect of the A/F ratio and no trend was observed. The engine speed clearly reduced the phase of flame development independently of the load condition. The decrease in the flame development phase was verified by absolute values, but only for 1000 r/min.

For the fast burn and final phase of the combustion, the increasing A/F ratio induced a longer duration for each phase in terms of ºCA. However, it was possible to verify some conditions for the 50 Nm load in which this trend was not confirmed. A/F ratio was verified to present more effects on the second half of the fast burn period (CA50 to CA90).

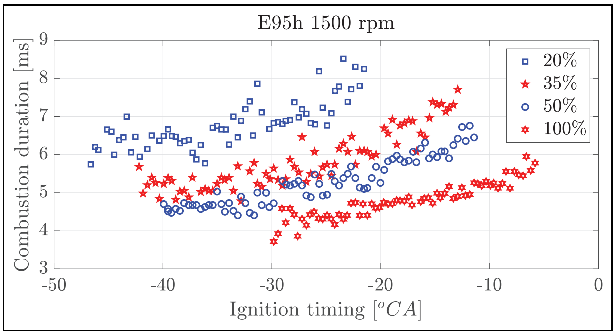

Figure 5. Combustion duration for different loads and ignition timing at 1500 r/min.

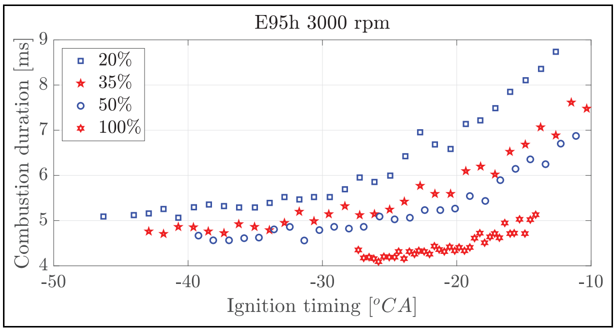

Figure 6. Combustion duration for different loads and ignition timing at 3000 r/min.

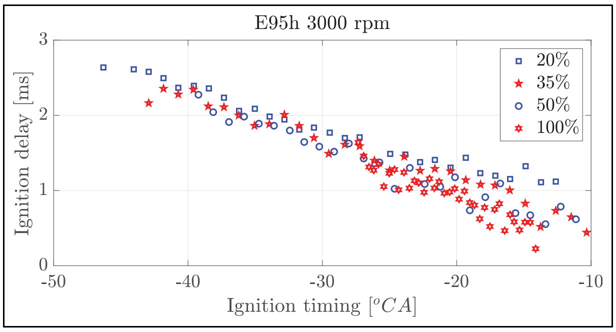

Figure 7. Ignition delay for different loads and ignition timing at 3000 r/min.

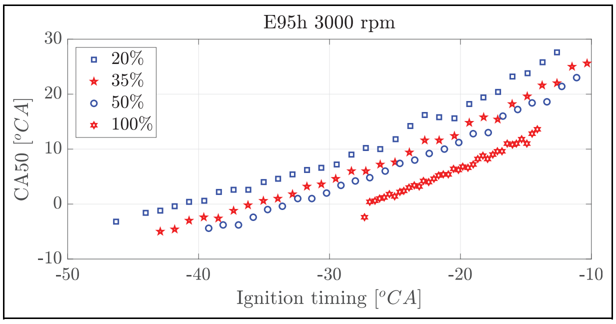

Figure 8. CA50 for different loads and ignition timing at 3000 r/min.

The overall fast burn phase participation in the combustion duration presented a reduction with increased engine speed. In relative terms, the effect of the A/F ratio on fast burn phase was not clearly observed for 25 Nm. For the 50 Nm condition, the stoichiometric condition presented the lowest share of the fast burn phase in combustion. However, there was no direct relation between the duration of fast burn phase and the A/F ratio as the condition $\lambda = 1.2$ presented the longest fast burn phase and $\lambda = 1.3$ presented the second longest duration for the fast burn phase.

The final phase of combustion presented no relation to the A/F ratio, but was increased with increases in engine speed for both 25 and 50 Nm.

Effect of ignition timing

A large variability was observed in the results for low engine speed (Figures 5 and 6). Owing to the great variability presented by the condition of 1500 r/min of engine speed and to the similarity found in the results for this condition, the results are presented only for 3000 r/min. The combustion duration presented a decrease for high loads owing to higher in-cylinder pressure. Moreover, the late ignition timing induced a higher combustion duration in an exponential relation, similar to the results found by Liu et al.[49] for engines fueled with gasoline.

The ignition delay presented a significant relation to ignition timing and was slightly influenced by load (Figure 7). As ignition was retarded, the pressure and temperature of the reactants were higher and, therefore, the period of flame kernel development was decreased in a linear relation to the ignition timing.

CA50 presented an almost linear relation to the ignition timing (Figure 8). This trend was a result of the effect of the late SOC due to late ignition timing increased combustion duration caused by late ignition timing (Figure 6). Therefore, it was possible to verify a relation between CA50 and combustion duration (Figure 9).

Aleiferis et al.[47] indicated that the position of CA50 and the pressure peak location can be used as an approximation for the MBT. Although industries apply some empirical rules to determine the location of the optimum CA50,[48] different values were found: approximately 6ºCA ATDC for the optimum CA50 against the 10 ºCA ATDC provided by the literature and a pressure peak located at 12°CA against the 16 ºCA ATDC provided by the literature. Those results corroborate the conclusions of De Oliveira Carvalho et al.[50]

The relation between ignition timing and indicated mean effective pressure (IMEP) is well established in the literature. There is an optimum value for ignition timing as late combustion is longer, decreasing the rate of heat release whereas early combustion increases the

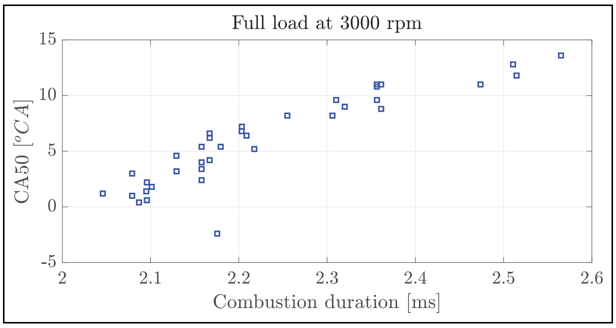

Figure 9. Relation between CA50 and combustion duration.

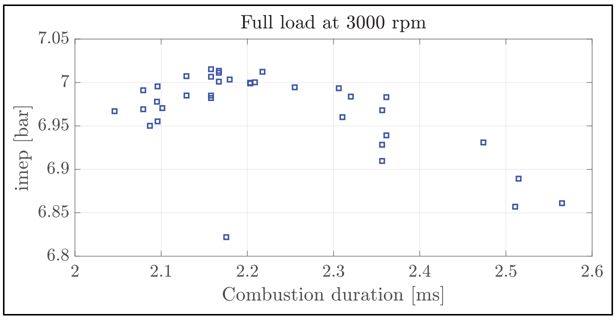

Figure 10. Relation between IMEP and combustion duration.

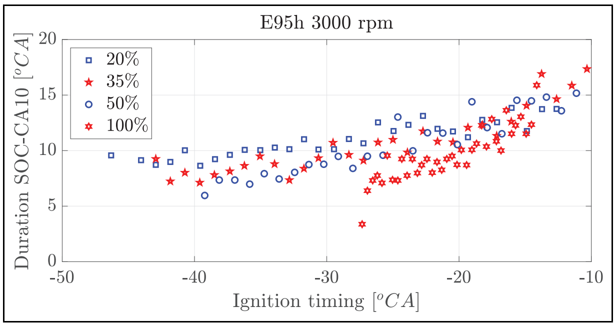

Figure 11. Absolute initial phase of combustion for 3000 r/min.

pressure during the compression stroke, generating negative power[42] (Figure 10). It was verified that the IMEP is reduced for faster combustion since the ignition time was too advanced, indicating that IMEP was not only a function of combustion duration but also of combustion phasing.

Load presented a negligible influence on the flame development in terms of ºCA (Figure 11).

The beginning of the fast burning phase presented a relation to ignition timing, whereas it presented no relation to load (Figure 12). The final part of the fast burning phase presented no relation to the ignition timing for the full load condition only (Figure 13). The overall fast burn phase was increased with respect to the ignition timing (Figure 14).

The final phase of the combustion presented an increase (Figure 15). The results indicated that the effect

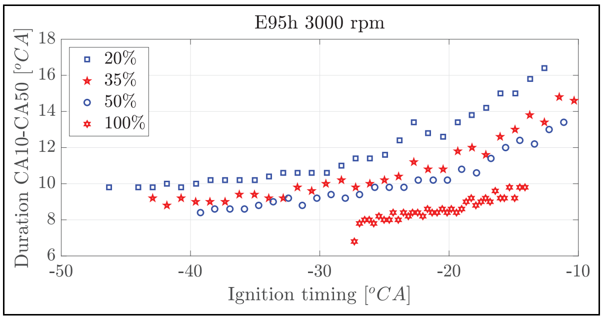

Figure 12. Absolute beginning of fast burn phase of combustion for 3000 r/min.

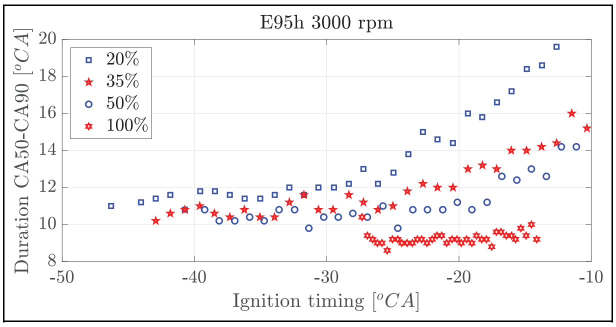

Figure 13. Absolute end of fast burn phase of combustion for 3000 r/min.

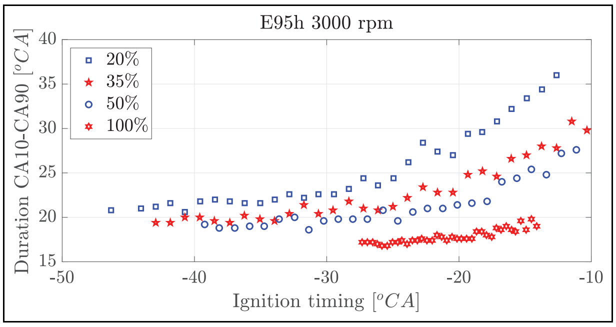

Figure 14. Absolute fast burn phase of combustion for 3000 r/min.

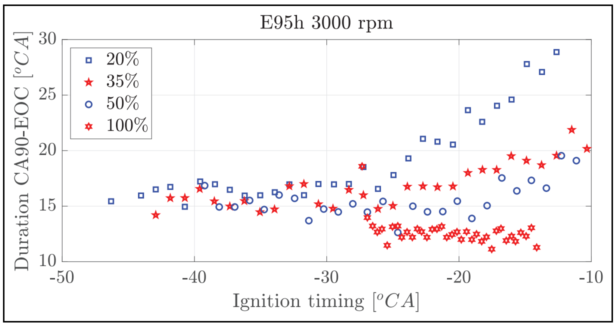

Figure 15. Absolute final phase of combustion for 3000 r/min.

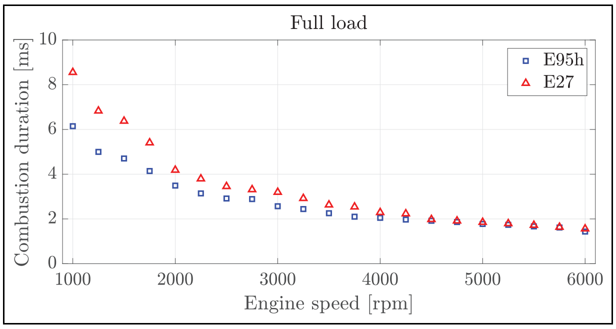

Figure 16. Comparison between combustion duration of ethanol and gasohol for different speed at full load.

of retarding ignition timing induced a longer initial phase of combustion. These results were unexpected as the flame development phase should be shortened by retarding the ignition timing owing to the increased pressure and temperature at the SOC,[51] similar to the trend observed for ignition delay. One hypothesis is that the implemented algorithm could not identify the SOC precisely and, thus part of the flame development was being accounted for as the ignition delay.

Comparison between ethanol and gasohol for full load condition

A comparison between the combustion durations for ethanol and gasohol is presented for a full–load condition (Figure 16). As expected, ethanol presented a shorter combustion duration than gasohol, confirming the remarks in the literature. The heat of vaporization of ethanol is higher than that of gasohol, leading to a lower temperature for the ethanol–air mixture. Although low temperatures caused a decrease in flame speed, the effect of the ethanol combustion chemistry prevailed over the temperature effects as the turbulent flame speed of ethanol is significantly higher than that of gasoline for combustion under engine conditions.[5,9,52]

The effects of charge cooling owing to fuel vaporization can be verified even in PFI engines, in which the air–fuel mixture is formed outside the cylinder. The high resistance of ethanol to knock onset is due to the high vaporization enthalpy, resulting in a colder air–fuel mixture than that of gasohol at the beginning of the combustion.[53,54] In addition, the shorter combustion of ethanol compared to that of gasohol prevents the autoignition being achieved. Consequently, the difference between the combustion durations of ethanol and gasohol was more pronounced for engine speeds lower than 1750 r/min, owing to the ignition retarding conducted for gasohol to avoid knock onset.

The ECU calibration strategy predicted a late ignition timing for gasohol even for conditions in which the knock onset was not critical, that is, for values of engine speed higher than 2000 r/min. By combining the late ignition timing and the longer combustion duration, the CA50 parameter occurred late for gasohol (Table 4).

Table 4. Comparison between CA50 of ethanol and gasohol for different speed at full load.

Engine speed (r/min)	E95h	E27
1000	32	9
1250	32	11
1500	35	13
1750	30	12
2000	21	9

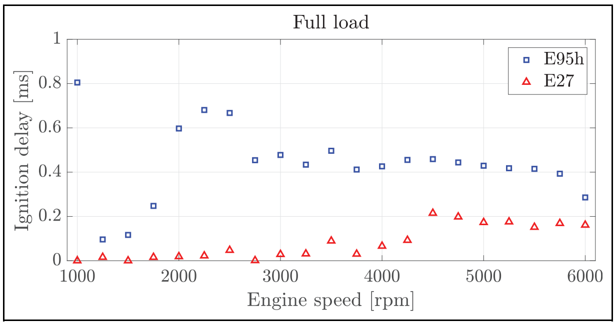

Figure 17. Comparison between ignition delay of ethanol and gasohol for different speed at full load.

The ignition delay presented lower values for gasohol than for ethanol (Figure 17). This result can be attributed to the low temperature of the ethanol–air mixture.

Ethanol presented a faster combustion as compared to that of gasohol in all of its phases, in absolute terms (Appendix 2, Tables 7 and 8). Although the ignition delay was longer for ethanol, the flame development presented a larger share of the combustion duration for gasohol.

The initial part of the fast burn was shorter for ethanol, whereas the final part of the fast burn was shorter for gasohol.

The share of the overall fast burn phase in the combustion duration, that is, fast burn duration in terms of percentage of total combustion duration was longer for ethanol owing to the its shorter flame development than that of gasohol. Ethanol molecules are simpler than those of gasoline, and thus less reactions are required to develop a flame.[55] Moreover, the fast burn phase of ethanol combustion was slightly influenced by engine speed, whereas the fast burn phase for gasohol presented a significant sensibility to engine speed.

The final phase of the combustion of gasohol presented a lower share of the combustion duration for engine speed above 2000 r/min. This results was caused by the late ignition timing for gasohol at low speeds, increasing the combustion duration. Consequently, the EOC occurred late in the expansion stroke, when the

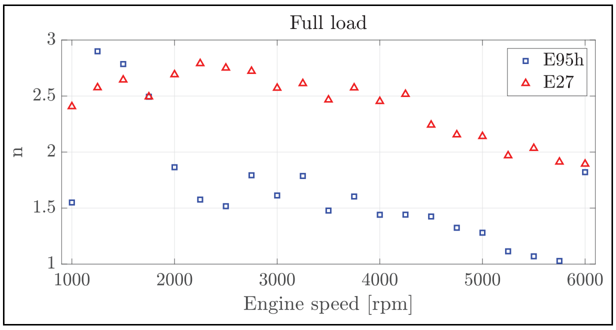

Figure 18. Comparison between form factor of ethanol and gasohol for different speed at full load.

pressure and temperature were reduced because of the increasing of combustion in the chamber volume.

Cooney et al.[25] found a similar trend for different compositions of gasohol, indicating that an increase of ethanol concentration decreases the length of the flame development phase. De Melo et al.[32] tested various blends of hydrous ethanol and gasoline in an engine operating at 3875 r/min and at two conditions of load: 60 and 105 Nm, demonstrating that a higher concentration of ethanol leads to an earlier peak of the HRR. The results regarding the contribution of each combustion phase found in this work corroborate the remarks of the literature. These results were caused by the difference in flame speed between both fuels. By fitting the Wiebe function using the method described in section 2, it was possible to verify the effect of combustion profile on the form factor n (Figure 18), which was constant for gasohol for low engine speed below 4250 r/min at 2.5 and decreased for high engine speed, attaining values near 2. This result agreed with the values provided by Mueller et al.,[34] who have found values between 2 and 2.7. A value of approximately 1.5 was observed for ethanol, decreasing to 1 for high engine speed. The characteristic of an early heat release profile for ethanol was also verified by comparing the values found for gasohol to those found for ethanol.

Conclusion

In this work, the effects of operational conditions on combustion of Brazilian ethanol were evaluated by analyzing parameters such as combustion duration, CA50, and form factor, as obtained from a two zone combustion diagnosis performed on experimental data from tests on a flexfuel SI engine. The combustion characteristics were explained using results from the literature and exposed the effects of the fuel properties, ignition timing, A/F ratio, load, and engine speed on the combustion. In addition, the combustion of ethanol was compared with the combustion of gasohol for an engine operating at wide open throttle condition under normal operation of the ECU, that is, with the ignition timing automatically controlled.

The verified influences of engine parameters on E95h combustion are summarized below.

- The engine speed has the most significant influence on the combustion because of the turbulence, whose increase leads to a faster flame propagation, and mainly affects the initial phases of combustion.
- Leaner mixtures increase the combustion duration. However, the A/F ratio only has a slight influence on combustion and it can be overlapped by the stochastic nature of combustion, mainly in high engine speed conditions.
- Ignition timing increases the combustion duration as it is retarded, although the ignition delay is reduced because of the higher in-cylinder temperature.
- The CA50 parameter is related to the MBT. However, its optimum value is not fixed for different types of fuel. Engine speed has a negligible effect on the optimum CA50 as the combustion duration presents a small variation in terms of crank angle.

A lean mixture strategy (for fuel economy) has conventionally been avoided, owing to issues regarding both emissions and combustion stability. For slightly lean conditions, that is, $\lambda = 1.1$, the NOx emission is increased.[23] For higher A/F ratios, the NOx emission is decreased, but the combustion is not stable enough to assure drivability when gasoline is used as fuel. The low sensibility to the air–fuel ratio presented by the ethanol indicates that ethanol is a promising alternative for lean mixture operation.

The comparison between the combustion of E95h and that of E27 showed that the former followed the same trend as the latter. The most evident difference between those fuels was that E95h presented faster combustions with faster phases of flame development and differences in the beginning of the fast burn phase. The difference among combustion durations was more significant at lower speeds, as the engine had to retard spark advance to avoid knock when running with E27. As combustion was being evaluated based on the Wiebe parameters, it is fundamental to consider not only combustion duration, but also the profile of the combustion. The exponent of the Wiebe function, n, is assumed to be 2 independently of the fuel. However, ethanol has a higher heat of vaporization compared to that of gasoline and thus, the in–cylinder temperature is lower at the SOC. Therefore, the ignition delay is greater and the beginning of the combustion is slower for ethanol, whereas it becomes faster during the fast burning period. This trend can be observed in the lower values of the form factor of the Wiebe function for ethanol.

Knowledge of the effects of engine parameters on the combustion of hydrous ethanol and the differences between hydrous ethanol and gasohol combustion can help improve the development and calibration of ECUs for flexfuel engines by providing information for simulation and engine research. Moreover, the values of combustion duration and Wiebe parameters are provided for a wide set of operational conditions, allowing for the use of this data for combustion modeling in engine simulation. Future work can provide comprehensive results for the effects of direct injection and compression ratio in ethanol combustion. Following the trends in engine research, the limits for lean operation of ethanol can be explored and the combustion parameters obtained from this type of analysis will indicate the feasibility of implementing such strategy in commercial engines.

Acknowledgements

The authors express their gratitude to Instituto Mauá de Tecnologia (IMT), its staff, and Professor Clayton Barcelos Zabeu for the execution of the experimental tests. The authors appreciate the equipment and technical support granted by PSA Citröen-Peogeot group. The authors also express their gratitude to Fundação de Amparo à Pesquisa do Estado de São Paulo (FAPESP) for the support provided through process No 2018/ 18859-1.

Declaration of conflicting interests

The author(s) declared no potential conflicts of interest with respect to the research, authorship, and/or publication of this article.

Funding

The author(s) disclosed receipt of the following financial support for the research, authorship, and/or publication of this article: This research was funded by the process no 2018/18859-1, Fundação de Amparo à Pesquisa do Estado de Sao Paulo (FAPESP)

ORCID iD

Caio H Rufino https://orcid.org/0000-0002-4564-5377

References

1. Guezennec YG and Hamama W. Two-zone heat release analysis of combustion data and calibration of heat transfer correlation in an I. C. engine. SAE paper 1999-01-0218, 1999.
2. Gatowski J, Balles E, Chun K, et al. Heat release analysis of engine pressure data. SAE paper 841359, 1984.
3. Abbaszadehmosayebi G and Ganippa L. Characterising Wiebe equation for heat release analysis based on combustion burn factor (C_i). *Fuel* 2014; 119: 301–307.
4. Brunt MF, Rai H and Emtage AL. The calculation of heat release energy from engine cylinder pressure data. SAE paper 981052, 1998.
5. Aleiferis P, Serras-Pereira J and Richardson D. Characterisation of flame development with ethanol, butanol, *iso*-octane, gasoline and methane in a direct-injection spark-ignition engine. *Fuel* 2013; 109: 256–278.
6. Eisazadeh-Far K, Moghaddas A, Al-Mulki J, et al. Laminar burning speeds of ethanol/air/diluent mixtures. *Proc Combust Inst* 2011; 33: 1021–1027.
7. Konnov AA, Meuwissen R and De Goey L. The temperature dependence of the laminar burning velocity of ethanol flames. *Proc Combust Inst* 2011; 33: 1011–1019.
8. Gülder ÖL. Burning velocities of ethanol-isooctane blends. *Combust Flame* 1984; 56: 261–268.
9. Aleiferis PG and Behringer MK. Flame front analysis of ethanol, butanol, iso-octane and gasoline in a spark-ignition engine using laser tomography and integral length scale measurements. *Combust Flame* 2015; 162: 4533–4552.
10. Ghojel J. Review of the development and applications of the Wiebe function: a tribute to the contribution of ivan Wiebe to engine research. *Int J Eng Res* 2010; 11: 297–312.
11. Yeliana Y, Cooney C, Worm J, et al. Estimation of double-Wiebe function parameters using least square method for burn durations of ethanol-gasoline blends in spark ignition engine over variable compression ratios and EGR levels. *Appl Therm Eng* 2011; 31: 2213–2220.
12. Bonatesta F, Waters B and Shayler P. Burn angles and form factors for Wiebe function fits to mass fraction burned curves of a spark ignition engine with variable valve timing. *Int J Eng Res* 2010; 11: 177–186.
13. Yeliana Y, Cooney C, Worm J, et al. Wiebe function parameter determination for mass fraction burn calculation in an ethanol-gasoline fuelled SI engine. *J KONES Powertrain Trans* 2008; 15: 567–574.
14. Li M, Zhang Q, Li G, et al. Experimental investigation on performance and heat release analysis of a pilot ignited direct injection natural gas engine. *Energy* 2015; 90: 1251–1260.
15. Rakopoulos D, Rakopoulos C, Papagiannakis R, et al. Combustion heat release analysis of ethanol or *n*-butanol diesel fuel blends in heavy-duty DI diesel engine. *Fuel* 2011; 90: 1855–1867.
16. Oh S, Min K and Sunwoo M. Real-time start of a combustion detection algorithm using initial heat release for direct injection diesel engines. *Appl Therm Eng* 2015; 89: 332–345.
17. Mittal M, Zhu G and Schock H. Fast mass-fraction-burned calculation using the net pressure method for real-time applications. *Proc IMechE Part D: J Automobile Engineering* 2009; 223: 389–394.
18. Ortiz-Soto EA, Lavoie GA, Martz JB, et al. Enhanced heat release analysis for advanced multi-mode combustion engine experiments. *Appl Energy* 2014; 136: 465–479.
19. Bueno A, Velásquez J and Milanez L. Exergy based diagnosis of in-cylinder diesel engine processes. SAE paper 2004-01-3258, 2004.
20. Depcik C, Jacobs T, Hagena J, et al. Instructional use of a single-zone, premixed charge, spark-ignition engine heat release simulation. *Int J Mech Eng Educ* 2007; 35: 1–31.
21. Reitz RD. Directions in internal combustion engine research. *Combust Flame* 2013; 160: 1–8.
22. Bae C and Kim J. Alternative fuels for internal combustion engines. *Proc Combust Inst* 2017; 36: 3389–3413.
23. Yoon SH and Lee CS. Lean combustion and emission characteristics of bioethanol and its blends in a spark ignition (SI) engine. *Energy Fuels* 2011; 25: 3484–3492.

24. Augoye A and Aleiferis P. Characterization of flame development with hydrous and anhydrous ethanol fuels in a spark-ignition engine with direct injection and port injection systems. SAE paper 2014-01-2623, 2014.
25. Cooney CP, Worm JJ and Naber JD. Combustion characterization in an internal combustion engine with ethanol-gasoline blended fuels varying compression ratios and ignition timing. *Energy Fuels* 2009; 23: 2319–2324.
26. Lanzanova TDM, Dalla Nora M and Zhao H. Performance and economic analysis of a direct injection spark ignition engine fueled with wet ethanol. *Appl Energy* 2016; 169: 230–239.
27. El-Faroug MO, Yan F, Luo M, et al. Spark ignition engine combustion, performance and emission products from hydrous ethanol and its blends with gasoline. *Energies* 2016; 9: 984.
28. Costa RC and Sodré JR. Hydrous ethanol vs. gasoline-ethanol blend: engine performance and emissions. *Fuel* 2010; 89: 287–293.
29. Costa RC and Sodré JR. Compression ratio effects on an ethanol/gasoline fuelled engine performance. *Appl Therm Eng* 2011; 31: 278–283.
30. De Melo TCC, Machado GB, De Oliveira EJ, et al. Different hydrous ethanol—gasoline blends—FTIR emissions of a flex-fuel engine and chemical properties of the fuels. SAE paper 2011-36-0080, 2011.
31. De Melo TCC, Machado GB, De Oliveira, Carvalho L, et al. In cylinder pressure curve and combustion parameters variability with ethanol addition. SAE paper 2012-36-0486, 2012.
32. De Melo TCC, Machado GB, Belchior CR, et al. Hydrous ethanol–gasoline blends —combustion and emission investigations on a flex-fuel engine. *Fuel* 2012; 97: 796–804.
33. Sileghem L, Vancoillie J, Demuynck J, et al. Alternative fuels for spark-ignition engines: mixing rules for the laminar burning velocity of gasoline–alcohol blends. *Energy Fuels* 2012; 26: 4721–4727.
34. Mueller RP, Li C and Tsao K. Modeling for mass burning rate and combustion duration in spark ignition engines using gasohol fuels. SAE paper 831677, 1983.
35. Brunt MF and Emtage AL. Evaluation of burn rate routines and analysis errors. SAE paper 970037, 1997.
36. Stone C and Green-Armytage D. Comparison of methods for the calculation of mass fraction burnt from engine pressure —time diagrams. *Proc IMechE Part D: J Automobile Engineering* 1987; 201: 61–67.
37. Ball J, Raine R and Stone C. Combustion analysis and cycle-by-cycle variations in spark ignition engine combustion part 1: an evaluation of combustion analysis routines by reference to model data. *Proc IMechE Part D: J Automobile Engineering* 1998; 212: 381–399.
38. Kamimoto T, Minagawa T and Kobori S. A two-zone model analysis of heat release rate in diesel engines. SAE paper 972959, 1997.
39. Catania A, Misul D, Mittica A, et al. A refined two-zone heat release model for combustion analysis in SI engines. *JSME Int J Series B Fluids Therm Eng* 2003; 46: 75–85.
40. Hohenberg GF. Advanced approaches for heat transfer calculations. SAE paper 790825, 1979.
41. Arhangel'skij VM, Hovah MS, Stepanov JA,, et al. *Motor vehicle engines*. Moscow: Mir Publishers, 1971.
42. Heywood JB. *Internal combustion engine fundamentals*. New York: McGraw-Hill, 1988.
43. Gallo W. *Análise Exergética de Motores a Gasolina e a Álcool*. PhD Thesis, Faculdade de Engenharia Mecânica, Universidade Estadual de Campinas, Campinas, Brazil, 1990.
44. Zabeu CB, Camargos LC, Marinsek LR, et al. Influence of injection timing on the engine efficiency and emissions in a si pfi engine using ethanol-gasoline blends with several water content levels. SAE paper 2017-36-0147, 2017.
45. Smola AJ and Schölkopf B. A tutorial on support vector regression. *Stat Comput* 2004; 14: 199–222.
46. Varea E, Modica V, Vandel A, et al. Measurement of laminar burning velocity and Markstein length relative to fresh gases using a new postprocessing procedure: application to laminar spherical flames for methane, ethanol and isooctane/air mixtures. *Combust Flame* 2012; 159: 577–590.
47. Aleiferis P, Behringer M, OudeNijeweme D, et al. Insights into stoichiometric and lean combustion phenomena of gasoline–butanol, gasoline–ethanol, iso-octane–butanol, and iso-octane–ethanol blends in an optical spark-ignition engine. *Combust Sci Technol* 2017; 189: 1013–1060.
48. Schifter I, Diaz L, Rodriguez R, et al. Combustion and emissions behavior for ethanol–gasoline blends in a single cylinder engine. *Fuel* 2011; 90: 3586–3592.
49. Liu J, Zhu G, Fu J, et al. Quantitative study on in-cylinder combustion and heat release characteristic parameters of gasoline engine based on single variable sweeping tests. *Appl Therm Eng* 2017; 117: 487–500.
50. De Oliveira Carvalho L, De Melo TCC and Neto RMDAC. Investigation on the fuel and engine parameters that affect the half mass fraction burned (CA50) optimum crank angle. SAE paper 2012-36-0498, 2012.
51. Serras-Pereira J, Aleiferis P and Richardson D. An analysis of the combustion behavior of ethanol, butanol, *iso*-octane, gasoline, and methane in a direct-injection spark-ignition research engine. *Combust Sci Technol* 2013; 185: 484–513.
52. Szybist JP and Splitter D. Effects of fuel composition on EGR dilution tolerance in spark ignited engines. *SAE Int J Eng* 2016; 9: 819–831.
53. Sluder CS, Szybist JP, McCormick RL, et al. Exploring the relationship between octane sensitivity and heat-ofvaporization. *SAE Int J Fuels Lubr* 2016; 9: 80–90.
54. Stein RA, Polovina D, Roth K, et al. Effect of heat of vaporization, chemical octane, and sensitivity on knock limit for ethanol—gasoline blends. *SAE Int J Fuels Lubr* 2012; 5: 823–843.
55. Sarathy SM, Oßwald P, Hansen N, et al. Alcohol combustion chemistry. *Prog Energy Combust Sci* 2014; 44: 40–102.

Appendix 1

Notation

Roman

a	Wiebe asymptotic parameter, –
A	area, m^2
c_p	specific heat at constant pressure, $J/(kgK)$
c_v	specific heat at constant volume, $J/(kgK)$
h	intensive enthalpy, J/kg
h^{HT}	coefficient of heat transfer, $W/(m^2K)$
H	enthalpy, J
L	auxiliary variable, –

LHV	lower heating value, J/kg
m	mass, kg
n	Wiebe exponent, –
P	pressure, Pa
Q	heat, J
R	gas constant, J/(kgK)
T	temperature, K
U	internal energy, J
V	volume, m^3
W	work, J
X_b	mass fraction burned, –

Greek symbol

$\Delta\theta$	combustion duration, $°CA$
η	maximum MFB, –
λ	relative air–fuel ratio, –
θ	crank position, $°CA$
ω	angular velocity, rad/s

Subscripts

$fuel$	fuel
p	combustion products
r	reactants
w	cylinder wall
0	start of combustion
10	10% of MFB
50	50% of MFB
90	90% of MFB

Appendix 2

Combustion duration tables

Table 5. Duration of each combustion phase for 25 Nm.

Engine speed (r/min)		1000				2000				3000				4000			
λ		1.0	1.1	1.2	1.3	1.0	1.1	1.2	1.3	1.0	1.1	1.2	1.3	1.0	1.1	1.2	1.3
2SOC—CA10	Abs	9	7	7	6	6	6	6	6	5	4	5	6	3	4	5	5
	Norm	16	12	9	7	9	8	6	6	7	5	6	7	4	5	6	5
*CA10—CA50	Abs	10	12	14	15	12	14	15	16	11	12	13	14	10	11	12	15
	Norm	18	18	17	16	18	17	15	15	15	14	15	16	13	14	15	14
*CA50—CA90	Abs	14	16	20	25	18	21	26	29	19	22	22	24	20	21	22	28
	Norm	24	26	26	26	26	27	26	26	26	26	26	26	26	26	26	26
*CA10—CA90	Abs	24	28	34	40	30	35	41	46	30	33	35	38	31	32	34	42
	Norm	43	44	44	42	44	43	42	41	41	40	41	42	39	40	41	40
*CA90—EOC	Abs	24	28	37	49	33	39	51	58	38	45	45	46	44	45	44	58
	Norm	41	45	47	51	47	49	53	53	52	54	53	51	56	55	53	55

SOC: start of combustion; EOC: end of combustion.

Table 6. Duration of each combustion phase for 50 Nm.

Engine speed (r/min)		1000				2000				3000				4000			
λ		1.0	1.1	1.2	1.3	1.0	1.1	1.2	1.3	1.0	1.1	1.2	1.3	1.0	1.1	1.2	1.3
2SOC—CA10	Abs	10	9	9	–	6	7	7	8	4	5	6	7	3	5	6	6
	Norm	21	20	18	–	9	11	10	9	7	6	9	8	4	6	9	6
*CA10—CA50	Abs	9	9	10	–	11	12	13	15	10	11	12	14	10	11	12	14
	Norm	19	20	20	–	17	18	18	18	15	15	17	17	12	15	17	15
*CA50—CA90	Abs	11	11	12	–	17	17	19	23	17	19	19	22	22	20	19	24
	Norm	23	24	25	–	26	26	26	26	26	26	26	27	25	26	26	26
*CA10—CA90	Abs	21	20	22	–	27	29	32	38	27	30	32	36	32	31	31	38
	Norm	43	45	45	–	42	44	45	44	41	41	44	43	37	41	43	41
*CA90—EOC	Abs	17	16	18	–	31	29	32	40	34	38	34	41	50	41	35	48
	Norm	36	36	37	–	49	45	45	47	52	53	47	49	59	53	48	53

SOC: start of combustion; EOC: end of combustion.

Table 7. Duration of each combustion phase for ethanol at full load condition.

Engine speed (r/min)		1000	2000	3000	4000	5000	6000
SOC—CA10	Abs	7	10	9	9	8	12
	Norm	19	23	20	18	16	23
CA10—CA50	Abs	8	9	10	10	11	11
	Norm	21	21	21	21	20	21
CA50—CA90	Abs	9	10	11	12	13	12
	Norm	24	23	24	25	25	23
CA10—CA90	Abs	17	19	21	22	24	23
	Norm	46	45	45	46	45	45
CA90—EOC	Abs	13	14	16	18	21	17
	Norm	35	32	35	37	39	33

SOC: start of combustion; EOC: end of combustion.

Table 8. Duration of each combustion phase for gasohol at full load condition.

Engine speed (r/min)		1000	2000	3000	4000	5000	6000
SOC—CA10	Abs	15	16	18	16	15	13
	Norm	29	32	31	30	26	23
CA10—CA50	Abs	11	11	13	12	12	12
	Norm	22	22	22	22	22	21
CA50—CA90	Abs	10	10	12	12	12	13
	Norm	20	20	20	21	22	23
CA10—CA90	Abs	22	21	24	24	24	25
	Norm	42	41	42	43	44	45
CA90—EOC	Abs	15	13	16	15	17	18
	Norm	29	27	27	27	30	32

SOC: start of combustion; EOC: end of combustion.